Available online at www.sciencedirect.com

ScienceDirect

Geochimica et Cosmochimica Acta 303 (2021) 1–14

Geochimica et Cosmochimica Acta

www.elsevier.com/locate/gca

On calcium-to-alkalinity anomalies in the North Pacific, Red Sea, Indian Ocean and Southern Ocean

Zvi Steiner [a,b,*], Amit Sarkar [c], Xuewu Liu [d], William M. Berelson [e], Jess F. Adkins [f], Eric P. Achterberg [a], P. Sabu [c], Satya Prakash [g], P.N. Vinaychandran [h], Robert H. Byrne [d], Alexandra V. Turchyn [b]

[a] *GEOMAR Helmholtz Centre for Ocean Research Kiel, Wischhofstr. 1-3, 24148 Kiel, Germany*
[b] *Department of Earth Sciences, University of Cambridge, CB2 3EQ Cambridge, UK*
[c] *National Centre for Polar and Ocean Research, Ministry of Earth Sciences, Goa, India*
[d] *College of Marine Science, University of South Florida, Saint Petersburg, Florida, USA*
[e] *University of Southern California, Los Angeles, CA 90089, USA*
[f] *California Institute of Technology, Pasadena, CA 91125, USA*
[g] *Indian National Centre for Ocean Information Services, Hyderabad, India*
[h] *Indian Institute of Sciences, Bangalore, India*

Received 29 May 2020; accepted in revised form 26 March 2021; available online 05 April 2021

Abstract

An important factor for predicting the effect of increased CO_2 on future acidification of the ocean is a proper understanding of the interactions controlling production and dissolution of calcium carbonate minerals ($CaCO_3$). The production and dissolution of $CaCO_3$ in the ocean can be assessed over large spatial scales by measuring seawater calcium concentrations and total alkalinity (A_T), yet past studies suggest that there could be large discrepancies between calcium and A_T-based balances of the $CaCO_3$ cycle in the North Pacific and Indian Oceans. Here, we analyse water column samples collected along transects in the North Pacific, Southern Ocean, tropical Indian Ocean and Red Sea for their concentrations of calcium, nutrients, and A_T. We find that there is an excess calcium over A_T anomaly in the top 1000 m of the tropical Indian Ocean water-column. The source of this anomaly is the dissolution of subsurface gypsum deposits in the Red Sea. We find no evidence for calcium-over-A_T anomalies in the North Pacific, in contrast to previous studies. Our results show that, in most cases, calcium and A_T data agree well and can be used to reconstruct the marine $CaCO_3$ cycle.

Keywords: Calcium; Alkalinity; Ocean acidification; $CaCO_3$; Alkalinity anomaly; Carbonate cycle

1. INTRODUCTION

Over the recent past, large and increasing amounts of CO_2 have been emitted to the atmosphere as a result of fossil fuel burning. A significant portion of this CO_2 is absorbed by the ocean, causing continuous acidification of seawater and increased calcium carbonate mineral ($CaCO_3$) dissolution, mitigating the amount of CO_2 that accumulates in the atmosphere (Doney et al., 2009; Sulpis et al., 2018; Gruber et al., 2019). It is predicted that the oceans will ultimately, over the course of the next few millennia, absorb the majority of anthropogenic CO_2 via enhanced dissolution of $CaCO_3$ and downwelling of seawater enriched with CO_2 in high latitudes (Feely et al., 2004;

* Corresponding author at: GEOMAR Helmholtz Centre for Ocean Research Kiel, Wischhofstr. 1-3, 24148 Kiel, Germany.
E-mail address: zsteiner@geomar.de (Z. Steiner).

https://doi.org/10.1016/j.gca.2021.03.027
0016-7037/

Archer et al., 2009; Ilyina and Zeebe, 2012). To predict where and how quickly the ocean will assimilate the excess anthropogenic CO_2, it is crucial to understand what governs the dissolution of $CaCO_3$ (Subhas et al., 2017; Sulpis et al., 2017; Steiner et al., 2019; Boudreau et al., 2020). Previous calculations have suggested that dissolution in the water column should be less important than dissolution within surface sediments, which occurs over much longer timescales (Jansen et al., 2002; Sulpis et al., 2018). There is, however, growing evidence that $CaCO_3$ dissolution occurs both in the water column and in surface sediments (Betzer et al., 1984; Byrne et al., 1984; Milliman et al., 1999; Sabine et al., 2002; Berelson et al., 2007; Honjo et al., 2008; Cao and Dai, 2011; Keil, 2017; Buitenhuis et al., 2019). This evidence comes from measurements of seawater total alkalinity (A_T) as a proxy for increasing dissolved calcium concentrations due to $CaCO_3$ dissolution, and comparison of settling $CaCO_3$ particle fluxes at different depths. However, the A_T of seawater is also affected by processes other than the precipitation and dissolution of $CaCO_3$, and comparisons of settling material from the surface water, through intermediate waters and onto the oceanic seafloor involve processes that operate on very different timescales, and are affected by lateral deep-water movement.

The most direct way to quantify the extent of $CaCO_3$ dissolution is to monitor the calcium ion concentrations in the ocean (Cao and Dai, 2011). Most investigators choose not to follow this route due to the analytical challenges of distinguishing variability in calcium concentrations of <1% over a very large background, and the fact that seawater calcium concentrations change mostly as a function of salinity. The popular approach for quantifying $CaCO_3$ precipitation and dissolution is by measuring changes in A_T based on the assumption that A_T change by 2 moles for every mol of $CaCO_3$ precipitated or dissolved (e.g. Feely et al., 2002; Berelson et al., 2007; Fry et al., 2015; Takahashi et al., 2014). The difficulty with using A_T for this task is that, since A_T is the budget of all weak acids and bases in a water sample, it is affected by all electron transfer reactions, in particular the oxidation of organic matter (Dickson, 1981):

$$\begin{aligned} A_T = {} & [HCO_3^-] + 2[CO_3^{2-}] + [B(OH)_4^-] + [OH^-] \\ & + [HPO_4^{2-}] + 2[PO_4^{3-}] + [Si(OH)_3^-] \\ & + [NH_3] + [\text{organic acids}] + [HS^-] - [H^+]_f \\ & - [HSO_4^-] - [HF] - [H_3PO_4] \ldots \end{aligned} \quad (1)$$

There is a wealth of published data on parameters governing carbonate chemistry in the oceans (e.g. Feely et al., 2004; Sabine et al., 2004; Jiang et al., 2014; Takahashi et al., 2014; Fry et al., 2015; Olsen et al., 2020) but few published profiles of calcium concentrations. Published profiles reveal that there are small but measurable variations of the oceanic calcium concentrations with depth and among different ocean basins, beyond those accounted for by Forchammer's-Marcet's principle of constant relative proportions (Tsunogai et al., 1973; Horibe et al., 1974; Sen Gupta et al., 1978; Shiller and Gieskes, 1980; Krumgalz, 1982; Sen Gupta and Naqvi, 1984; Lebrato et al., 2020); this implies fast chemical reaction rates or large fluxes, as the residence time of calcium in the ocean is nearly one million years. Existing data also suggest that there is a persistent discrepancy between the relative changes in calcium concentrations and A_T, compared to the expectation that $CaCO_3$ reactions should add/remove A_T and calcium at a ratio of 2:1. Often the measured calcium concentrations are higher than would be expected from the measured changes in A_T or salinity (Naqvi and Naik, 1983; de Villiers, 1998; Roson et al., 2016).

Discrepancies in the difference between measured dissolved calcium and A_T imply that there could be gaps in our understanding of the cycling of inorganic carbon and large errors in predictions and estimates of the effects of ocean acidification. It has been shown that, in the surface mixed layer, ~20% of the particulate calcium and strontium (material that does not pass through a filter with nominal pore-size of 1 μm) is adsorbed to organic matter, providing a source of variability in the difference between dissolved calcium and A_T, if dissolved calcium is removed from seawater by this process (Bishop et al., 1977; Bishop et al., 1978). An alternate explanation for the measured discrepancies between calcium and A_T-based estimates of the marine $CaCO_3$ cycle is the hydrothermal hypothesis (de Villiers, 1998; de Villiers and Nelson, 1999). This hypothesis suggests that circulation of seawater through low-temperature hydrothermal systems produces widespread excess calcium anomalies at water depths of 1500–4000 m in the Pacific Ocean. Despite suggestions that there may be large scale discrepancies between the concentration of calcium and A_T in the Indo-Pacific Ocean, this question has never been systematically addressed.

In this study, we seek to re-evaluate the calcium and A_T cycles, and identify whether there are widespread discrepancies between estimates of $CaCO_3$ dissolution based on changes in calcium and A_T. As far as such discrepancies do exist, we seek to identify the causes of these discrepancies. The focus is on the North Pacific and Indian Oceans since these are the two oceanic regions for which previous studies reported the existence of excess calcium anomalies. The Southern Ocean is the common source of deep water to the Pacific and Indian Oceans, and the Red Sea is a source of Indian Ocean intermediate water. Inclusion of the Southern Ocean and Red Sea data serves to test whether excess calcium anomalies originate from the formation of distinct water masses.

2. MATERIALS AND METHODS

2.1. Sampling

North Pacific samples were collected on cruise CDisK-IV from Hawaii to Alaska, on board the RV Kilo Moana, in the period 01–30 August 2017 (Fig. 1). Samples for A_T were collected in clear BOD (Biochemical Oxygen Demand) borosilicate bottles (Fisher Scientific) and analysed onboard, shortly after sample collection (Naviaux et al., 2019). Each sample bottle was rinsed three times with seawater taken directly from a Niskin bottle through silicone tubing; each rinse volume was approximately

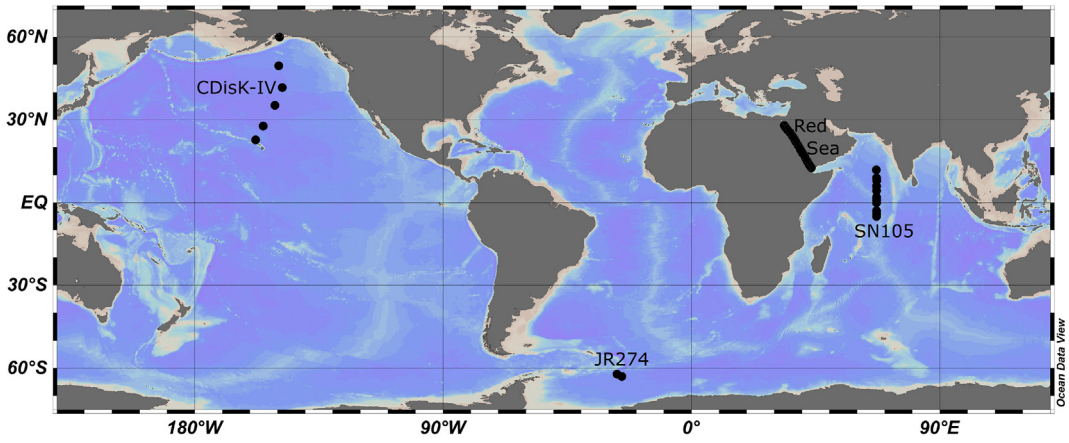

Fig. 1. Sampling locations and cruise names. Map plotted using ODV 5.3.0 (Schlitzer, 2020).

one-third of the sample-bottle volume. The tubing was then inserted at the bottom of the sample bottle and filled to overflowing; the overflow volume was approximately equal to the bottle volume. The sample temperature (required to ascertain bottle volume and to convert sample volume to sample mass) was measured to better than 0.1 °C using a digital thermometer. The tubing was then jostled up and down in the seawater sample to ensure that no air bubbles were trapped in the bottle. Once all bubbles were eliminated, the bottle cap was rinsed with seawater and the bottle was sealed with a ground glass stopper. Seawater in the flange area was eliminated and the bottleneck area was dried with a Kimwipe. Samples for nutrient analyses were filtered and kept frozen at −20 °C in polypropylene (PP) vials until analysis. Samples for cation concentrations and strontium isotopes were filtered through Millipore polyethersulfone (PES) syringe filters of nominal pore size of 0.22 µm into acid washed low density polyethylene (LDPE) bottles, acidified to pH = 1.7 with distilled nitric acid and kept refrigerated until analyses.

Tropical Indian Ocean samples were collected during cruise SN105 on board the ORV Sagar Nidhi from Goa to Mauritius. Samples were retrieved from 12°N to 5°S along 67°E in the period 07–16 December 2015. Water samples were drawn directly from PVC Niskin bottles mounted on a rosette sampler equipped with a CTD probe and the sampling bottles were rinsed three times with the water before the bottles were sealed. Nutrient samples were kept frozen at −18 °C in PP vials until analysis and measured onboard. Samples for A_T were stored in 60 mL amber glass bottles, poisoned with 30 µL of a saturated mercuric chloride solution and analysed after the cruise. Samples for cations were filtered through Millipore Polyvinylidene fluoride (PVDF) syringe filters of nominal pore size of 0.22 µm, and kept in PP vials at 4 °C until analysis. Temperature, conductivity and pressure were measured during the rosette casts using a 911plus CTD system (Sea-Bird Electronics, Bellevue, WA).

Southern Ocean samples were collected in the period between 9th January and 12th February 2013, during the UK ocean acidification cruise JR274 on board the RRS James Clark Ross. Samples for A_T were collected in 250 mL Schott glass bottles and poisoned with 50 µL of a saturated mercuric chloride solution (Tynan et al., 2016). Samples were immediately sealed and stored in the dark until analysis. Nutrient samples were collected in PP vials and analysed on-board, shortly after samples collection. Seawater samples destined for calcium concentration analyses were sampled with trace metal clean samplers, filtered through cartridge filters (0.2 µm Sartobran P300, Sartorius), and stored in 125 mL LDPE bottles (Nalgene). The samples were acidified on-board with ultra-clean HNO_3 to pH = 1.7 (Schlosser et al., 2018).

Red Sea surface water samples were collected in the period between 27th December 2015 and 3rd January 2016. Details of the analytical methods and results were published by Steiner et al. (2018). The samples were collected with a plastic bucket lowered from the deck of a container ship using a synthetic rope, and kept refrigerated in gas-tight plastic bottles until they were subsampled at the Israel Oceanographic and Limnological Research (IOLR) within three days of sampling. Samples for A_T were filtered through Whatman GFF 0.45 µm filters, transferred to amber brown glass bottles, and analysed at IOLR by potentiometric Gran titration. Samples for cation concentrations and strontium isotopes were kept in PP tubes and analysed at the University of Cambridge along with samples from the other cruises. Data from a full oceanographic station at 26.90°N, 34.77°E visited on 2 February 1982 are from Krumgalz and Erez (1984) and Krumgalz et al. (1990).

2.2. Alkalinity

2.2.1. Pacific Ocean alkalinity

Total alkalinity was measured spectrophotometrically on the North Pacific cruise using an Ocean Optics 4000 spectrophotometer, using bromocresol purple (BCP) as a pH indicator, following the method of Liu et al. (2015). In the ship's laboratory, the outside of each bottle was carefully rinsed with tap water to remove any salt and the bottle surface was wiped clean with Kimwipes. Samples were allowed to warm up to above 15 °C before analysis.

For the titration procedure, the sample bottle was anchored with a bottle holder on a stir plate. The bottle

cap was removed and rinsed into the sample bottle with a small amount (about 1 mL) of deionised (MilliQ, Millipore) water. A small magnetic stirrer bar was inserted into the bottle, and stirring commenced. The acid tube from the Dosimat titrator, inserted just below the surface of the sample liquid, ensures that the HCl is well mixed with the seawater before reaching the light path at the lower part of the bottle. After a reference absorbance was taken across the spectrum, the absorbances at 432, 589 and 730 nm were recorded, and 0.1 mL of the BCP stock solution was added. Acid was then delivered to the sample bottle, with the rate of acid addition being guided by continuous spectrophotometric monitoring of the seawater pH. The titrations were terminated at $R = 0.070$ (pH $\sim$ 4.2), where R is the absorbance ratio of the protonated and deprotonated BCP at the wavelengths 589 nm and 432 nm, respectively. The 730 nm wavelength was used to check the baseline shift. A fritted glass purging tube was then placed into the bottle above the light path and the solution was vigorously purged with N_2 until R was constant (0.002 unit in one minute ($\sim$5 min)). Finally, the temperature (0.01 °C precision) of the solution was measured with a digital thermometer and the final R ratio obtained at this temperature was used to obtain the final pH_T used for calculation of seawater A_T according to:

$$A_T = \frac{([HCl] \cdot V_A - [H^+]_{ASW} \cdot M_{ASW})}{M_{SW}} \quad (2)$$

where the sample mass (M_{SW}) is obtained by using a sample bottle of certified volume. The M_A term in M_{ASW} ($M_{ASW} = M_{SW} + M_A$) is determined by measuring the volume and density of the acid. The acid concentration, [HCl], is volume-based and is calibrated with certified reference material (CRM) provided by Dr Andrew Dickson (Scripps Institute of Oceanography, La Jolla, CA). V_A is the volume of acid delivered by the Dosimat titrator, and $M_A = V_A \sigma_A$ where σ_A is the density of the acid. Precision of the analyses is ± 3 μmol kg^{-1} based on analyses of duplicate samples.

2.2.2. Southern Ocean alkalinity

Samples from the Southern Ocean were analysed for A_T using a VINDTA 3C instrument. A Dickson CRM (Batches no. 119 & 120, Scripps Institute of Oceanography, La Jolla, CA) was titrated to determine the exact concentration of the titration acid. 1σ SD of the analyses was ± 2 μmol kg^{-1} based on the analyses of duplicate samples (Tynan et al., 2016).

2.2.3. Indian Ocean alkalinity

Total alkalinity was determined at the Hebrew University of Jerusalem by titration of duplicate 11 g samples filtered through PVDF syringe filters with a nominal pore size of 0.22 μm (Millex-GV). Titrations were performed with 0.05 N HCl in pure water at 25 °C using a TIM865 auto-sampler equipped with pHC2401-8 pH electrode (Radiometer Analytica). Calculations of A_T from the titration data were performed using the Gran titration method (Sass and Ben-Yaakov, 1977). The average difference between duplicate analyses was 1 μmol kg^{-1} ($n = 102$). The exact concentration of the titration acid was determined by running CRM samples (Batches no. 138 & 147, Scripps Institute of Oceanography, La Jolla, CA).

The salinities of select samples from the Indian Ocean cruise were measured at the Inter University Institute for Marine Sciences in Eilat by a MS-310e Micro-Salinometer (RBR Limited, Ottawa, Canada) with precision of 0.002–0.003. Each sample was analysed in three cycles with fill time of 65 seconds and a flush time of 85 seconds. Calibration was achieved by running IAPSO standard seawater batch P157 and three internal standards. A consistency standard was run every six samples to correct for instrumental drift. A_T normalization of the Indian Ocean data to constant salinity was performed using the bottle data if available or a 5-point running average of the CTD data when bottle data were not available. Salinity normalization of A_T data from other cruises was done using the CTD data.

2.3. Nutrients

Soluble reactive phosphate (SRP) and total oxidised nitrogen (TON; nitrate + nitrite) in the North Pacific samples were analysed at the U. Maryland Nutrient Analytical Services Lab (Solomons, MD, USA). SRP, silicic acid, ammonium, nitrite and TON were determined in Indian Ocean samples using a SAN^{++} auto analyser (Skalar Analytical B.V., AA Breda, The Netherlands). The protocols for the analyses followed the recommendations from Skalar Methods issue 110810/MH/99262991. Nutrient samples collected from the Southern Ocean were analysed using a Skalar San^{plus} segmented flow auto analyser following Kirkwood (1996).

2.4. Cation concentrations

The concentrations of calcium, magnesium and sodium in samples from the North Pacific, Red Sea and Indian Ocean were analysed at the University of Cambridge using an Agilent Technologies 5100 ICP-OES (Inductively Coupled Plasma Optical Emission Spectroscopy) based on the Ca422.673, Mg279.078, Mg285.213, Na568.821 and Na589.592 spectral lines following procedures described by Schrag (1999) and de Villiers et al. (2002), and modified for use in seawater (Steiner et al., 2020). Samples from Southern Ocean cruise JR274 were analysed by the same analyst, using the same set of standards, at GEOMAR Helmholtz Centre for Ocean Research Kiel using a Varian-720 ICP-OES, based on the Ca317.933, Ca370.602 and Na330.237 spectral lines. Samples were diluted to the same salinity (average dilution factor of 1:83) and analysed in two-to-eight replicates using sample-standard bracketing. The ICP-OES measures intensity of all spectral lines simultaneously, hence element ratios eliminate much of the uncertainty associated with flow and plasma instability. This feature was used to remove the effect of salinity variations on sample concentrations, and avoid plasma instability errors, by calculating calcium and magnesium concentrations from the measured Ca/Na and Mg/Na. Element-to-sodium ratios are multiplied by 0.46847 mol kg^{-1}, and by the ratio of measured practical salinity to

the calculated absolute salinity (IOC et al., 2010; McDougall and Barker, 2011). This operation normalizes calcium and magnesium concentrations to an absolute salinity of 35 g kg^{-1}, assuming that sodium-to-chlorinity and sodium-to-salinity ratios are constant in open ocean waters (Millero et al., 2008).

Precision of the calcium concentration analyses, calculated from duplicate analyses of all samples in the dataset, was 0.08% (8 µmol kg^{-1}) for the Indian Ocean and Red Sea samples (1σ SD, n = 172), 0.19% (19 µmol kg^{-1}) for the North Pacific samples (1σ SD, n = 188) and 0.08% (8 µmol kg^{-1}) for the Southern Ocean samples (1σ SD, n = 43). Calibration was performed by running an IAPSO standard from batch P157 at different dilutions. Calcium concentrations in the IAPSO standard were determined by Triton Plus Thermal Ionisation Mass Spectrometer (TIMS) after gravimetrically spiking IAPSO samples with a ^{42}Ca-^{48}Ca double spike, removing strontium from the spiked sample using Eichrom Sr resin and separating calcium from the remaining sample using an AG50W-X8 resin (Steiner et al., 2018). Calcium concentrations in IAPSO batch P157, normalized to absolute salinity of 35 g kg^{-1}, is 10.180 ± 0.010 mmol kg^{-1} according to this calibration.

2.5. Strontium isotopes

Strontium isotopic composition ($^{87}Sr/^{86}Sr$) was measured using a Triton Plus TIMS at the University of Cambridge, in the Department of Earth Sciences, to look for a geochemical signature of hydrothermal contributions. For each analysis, 300 ng strontium were separated from the seawater sample using Eichrom Sr resin. Instrumental mass fractionation was corrected by assuming $^{86}Sr/^{88}Sr = 0.1194$. Runs of the standard SRM987 alongside the samples yielded an $^{87}Sr/^{86}Sr = 0.710260 \pm 0.000009$ (2σ SE, n = 5).

3. WATER CHEMISTRY-BASED ESTIMATES OF $CACO_3$ DISSOLUTION

To account for conservative changes in the concentrations of A_T and calcium, those that are not related to $CaCO_3$ precipitation and dissolution, we normalize A_T and calcium concentrations to a constant salinity. We assume that changes to the salinity-normalized concentrations imply chemical reaction rather than dilution or concentration through evaporation. For example, for A_T this normalization is:

$$\text{Normalized } A_T(nA_T) = \frac{35 \cdot A_T}{S_A} \quad (3)$$

Absolute salinity (S_A) is calculated from the shipborne measurements of conductivity using the Gibbs-Seawater Oceanographic Toolbox (IOC et al., 2010; McDougall and Barker, 2011). Salinity normalization of the A_T data introduces errors when the intersect of the salinity-to-A_T curve deviates from zero due to non-conservative sources or sinks of A_T or if the zero-salinity end member is not equal to zero (Friis et al., 2003; Jiang et al., 2014; Fry et al., 2015). The magnitude of this error depends on the deviation from conservative behaviour and the deviation of the measured salinity from 35 g kg^{-1} (supporting information Table s1). The error introduced by normalization to salinity of 35 g kg^{-1}, when the absolute salinity is 34 or 36 g kg^{-1}, and A_T deviates by 150 µmol kg^{-1} from 2350 µmol kg^{-1}, is 4 µmol kg^{-1} (see Appendix 1 for the calculation). If A_T and calcium change non-conservatively due to $CaCO_3$ dissolution/ precipitation, salinity normalization introduces the same absolute charge equivalence error for both.

In the deep-sea, and in high-nutrient low-chlorophyll regions of the ocean, A_T is reduced by the production and release of nitrate, nitrite, soluble reactive phosphate (SRP), and sulfate during the oxidation of organic matter (Wolf-Gladrow et al., 2007). Brewer et al. (1975) have shown that changes in A_T due to the oxidation of organic matter can be accounted for by using measured nutrient concentration data. The nutrient-corrected (salinity-) normalized A_T is termed potential alkalinity (PA):

$$PA = \frac{\left(A_T + NO_3^- + NO_2^- + SRP + 2 \cdot SO_4^{2-}\right) \cdot 35}{S_A} \quad (4)$$

Sulfate released during the oxidation of organic matter changes A_T by a measurable amount (Kanamori and Ikegami, 1982) but variations in sulfate concentrations cannot be measured precisely enough due to the high background sulfate concentration. In calculation of the sulfate term in Eq. (4), we assume an average N:S ratio of 16:2.4 (Wolf-Gladrow et al., 2007). An additional term that contributes 4 µmol kg^{-1} to PA, on average, but is not included in our calculations, is organic alkalinity (Fong and Dickson, 2019). The organic alkalinity term is important in many coastal regions, but in the open ocean the distribution of organic alkalinity is poorly known and its variability likely small (Yang et al., 2015; Fong and Dickson, 2019). With the correction for nutrients and sulfate, some studies suggest that there is good agreement between variations in the concentrations of calcium and PA in the North Pacific (Kanamori and Ikegami, 1982). Other studies indicate that there are larger variations in calcium than PA, and that variability in the difference between calcium and A_T in the Pacific Ocean is driven by boundary processes such as hydrothermal basalt alteration, mixing with river water and authigenic formation of clay minerals (Shiller and Gieskes, 1980). Two decades later, de Villiers (1998) and de Villiers and Nelson (1999) presented what is likely the most internally consistent set of seawater calcium concentration measurements and suggested that there is a large-scale excess-calcium anomaly, of up to 50 µmol kg^{-1}, at depths of 1500–4000 m in the North Pacific Ocean. They defined excess-calcium as:

$$Ca_{ex} = \Delta n[Ca] - 0.5\Delta PA \quad (5)$$

where Δn[Ca] and ΔPA are the salinity-normalized calcium concentrations and potential alkalinity relative to their preformed North Atlantic Deep Water (NADW) or Antarctic Bottom Water (AABW) concentrations. This calculation assumed that the Southern Ocean end-member of calcium and A_T was well known and that the A_T data collected by GEOSECS, up to a few hundred miles from the collec-

tion sites of the samples, were sufficiently spatially homogenous to be compared (de Villiers, 1998). These authors hypothesized that the source of excess calcium anomaly is low-temperature hydrothermal activity. A similar excess calcium anomaly has been proposed in the Indian Ocean (Naqvi and Naik, 1983) but was not detected in the Atlantic Ocean (de Villiers, 1998; Roson et al., 2016), though data from the North Atlantic subtropical gyre suggest higher salinity-normalized calcium concentrations in AABW and AAIW (Antarctic Intermediate Water) compared to NADW (Roson et al., 2016).

To compare with past studies, we use the same definition of Ca_{ex} as given in Eq. (5). The combined uncertainty of the internal precision of PA calculated for samples from each ocean transect due to analytical noise, salinity normalizations, organic alkalinity, uncertainty in nutrient concentrations and nutrient ratios is 7 μmol kg^{-1}, calculated as the square root of the sum of the squared errors of the individual uncertainties (Orr et al., 2018). The salinity-normalization term cancels out in the calculation of Ca_{ex} since it affects PA and n[Ca] to a similar degree. The analytical uncertainty in the n[Ca] determination (8–20 μmol kg^{-1}) is larger than the precision error in PA calculation (PA is also divided by two in calculation of Ca_{ex}), and therefore dominates the error term of Ca_{ex}. The Southern Ocean end-member used for our calculations is the average of all calcium and PA determinations for Stations 43 & 44 on cruise JR274, normalized to an absolute salinity of 35 g kg^{-1} ($n[Ca] = 10.226 \pm 0.007$ mmol kg^{-1}, $PA = 2.406 \pm 0.027$ mmol kg^{-1}). These numbers produce Ca_{ex} values that are 47 μmol kg^{-1} lower than would be obtained using de Villiers's choice of the Southern Ocean end-members, which are $n[Ca] = 10.180$ mmol kg^{-1}, $PA = 2.409$ mmol kg^{-1} when normalized to the same absolute salinity (de Villiers, 1998).

The February 1982 Red Sea data do not include measurements of nutrient concentrations, hence PA was calculated based on apparent oxygen utilization, assuming a Redfield ratio of $P:N:C:-O_2 = 1:16:106:-138$. Nutrient data from the Red Sea suggest N:P ratios that are similar to this Redfield ratio or slightly higher, with significant spatial and temporal variability in the photic zone (Wafar et al., 2016; Kürten et al., 2019). Based on these data, application of the Redfield ratios introduces an error up to ±3 μmol kg^{-1} in the calculation of Ca_{ex} for data from the Red Sea.

The calculation used to assess the coherence of the calcium and PA data (Eq. (5)) corrects for three potential sources of variability: salinity, $CaCO_3$ precipitation or dissolution and photosynthesis or aerobic remineralization of organic matter. With the exception of water mass mixing, other processes that might impact the concentration of calcium or A_T are not routinely considered in marine studies. Among the many alternative mechanisms that could produce calcium-to-PA anomalies, five are more likely to be important on large spatial scales. The first is mixing between seawater and freshwater with high A_T or calcium relative to their sodium concentrations (Fry et al., 2015; Chakrabarti et al., 2018; Beckwith et al., 2019). A second potential mechanism that could influence the difference between dissolved calcium and A_T in seawater is anaerobic oxidation of organic matter. Aerobic oxidation of organic matter and denitrification, which slightly decrease A_T, are corrected using measured nitrate and SRP data. The oxidation of organic matter by manganese and iron oxides increases A_T (Froelich et al., 1979). Under more reducing conditions, microbial sulfate reduction can be a very large source of A_T if there is concurrent precipitation of iron sulfide minerals. A third mechanism that could alter the concentration of calcium and A_T is passage of large volumes of seawater through hydrothermal systems, resulting in water that is high in calcium, low in A_T and very low in magnesium (de Villiers, 1998; de Villiers and Nelson, 1999). The fourth and fifth mechanisms that could alter Ca_{ex} are adsorption of calcium by particulate organic carbon or detrital clay particles (Bishop et al., 1977; Bishop et al., 1978) and production of organic alkalinity from the incomplete oxidation of organic compounds (Yang et al., 2015; Ko et al., 2016). These processes are more likely to be important in coastal regions and highly productive regions of the ocean.

The null hypothesis tested in this work is that subsequent to normalization to a constant salinity, and correcting for water mass mixing and the contribution of aerobic organic matter remineralization to A_T, the concentrations of calcium and PA change only due to $CaCO_3$ precipitation and dissolution, that is $Ca_{ex} = 0$ (Eq. (5)). The single initial Ca_{ex} assumed for all water masses is derived from this definition of the null hypothesis. If the null hypothesis is correct, then this assumption is correct, regardless of the actual A_T and calcium concentration of the water mass. If the null hypothesis is incorrect, we would observe anomalies in calculated Ca_{ex} where the anomalous water mass is found.

3.1. Process studies

To assess the possibility that specific processes, such as river input and hydrothermal circulation, produce discrepancies between measured seawater calcium and A_T data, we take a closer look at ocean boundary regions. In the North Pacific, we analysed samples from Resurrection Bay, a fjord off the coast of Alaska that is continuously flushed by river water, to test whether Alaskan rivers are likely to produce Ca_{ex} anomalies (Eq. (5)) in the region by supplying weathering products and organic alkalinity. Samples from ocean Station ALOHA were analysed for radiogenic strontium isotopes and magnesium concentrations to identify hydrothermal contributions from the Hawaii volcanic chain. We expand our analyses to include data from the Red Sea, an important source of intermediate waters to the northern Indian Ocean. The Red Sea is a tectonically active, long and narrow basin with hot brine pools at its bottom. Evaporite deposits are dissolving at the bottom of the Red Sea and likely impact the calcium balance in the overlying water column (Craig, 1966). The absolute salinity of Red Sea waters is much higher than typical ocean water, exceeding 40 g kg^{-1}, allowing recognition of the Red Sea water mass in the Indian Ocean as a pronounced salinity maximum (Rochford, 1964; Wyrtki, 1973). Comparison of the Red Sea data with data from the tropical Indian

Ocean is designed to test the applicability of the hydrothermal hypothesis of de Villiers (1998) and de Villiers and Nelson (1999) to the Indian Ocean.

4. RESULTS

4.1. Ca_{ex} in the North Pacific and tropical Indian Ocean

The absolute changes in calcium and PA along the Hawaii to Alaska transect are very similar in terms of charge equivalence ($2 * \Delta[Ca^{2+}] = 1 * \Delta[PA]$). This equivalence is particularly close at the central stations 27°N, 35°N and 41°N (supplementary Fig. s1). There is no significant depth-dependent variation in Ca_{ex} within the North Pacific (Fig. 2).

Salinity-normalized calcium and PA in the tropical Indian Ocean increase from the surface to 2000 m by a similar number of charge equivalents. The fine details of the calcium and PA profiles reveal a disparity between the two parameters, with calcium concentrations increasing faster at shallow-to-intermediate depths, and PA increasing with depth at a steeper gradient than calcium below 1000 m. This creates an excess calcium anomaly between the upper 1000 m of the water column (Fig. 2; $\sigma_\theta < 27.5$, average $Ca_{ex} = 10 \pm 13$ μmol kg^{-1}) and depths from 1200 to 2000 m ($\sigma_\theta \geq 27.5$, average $Ca_{ex} = -5 \pm 8$ μmol kg^{-1}). A t-test rejects the hypothesis that the mean Ca_{ex} of samples from 0-1000 m and 1200–2000 m is the same, with $p = 0.0008$. The 95% confidence interval of the difference between Ca_{ex} of the shallower and deeper Indian Ocean samples is 8–22 μmol kg^{-1}. The distribution of the Ca_{ex} anomaly, as well as the existence of a corresponding salinity anomaly, suggest a possible origin for the excess calcium anomaly in the Red Sea and Persian Gulf water masses of the North Indian Ocean.

Potential alkalinity (PA) and calcium data from the North Pacific and tropical Indian Ocean are in good agreement with those of past studies (Fig. 3). Calcium analyses were done by the same analyst using water from a single batch of IAPSO standard for calibration and, thus, we believe they are consistent. Total alkalinity was analysed independently for each cruise.

4.2. Process studies

Calcium excess data from 50°N (Pacific Ocean Station Papa) initially suggest the possibility of a small negative Ca_{ex} anomaly (supporting Fig. s1). Average Ca_{ex} values in Resurrection Bay are similar to average Ca_{ex} values of the open waters of the North Pacific Ocean (3 ± 16 μmol kg^{-1} in Resurrection Bay, -2 ± 19 μmol kg^{-1} in the rest of the North Pacific dataset; Fig. 4D), suggesting that Alaskan Rivers are less likely to produce Ca_{ex} anomalies in the North Pacific.

Calcium excess data also show a small positive anomaly at the southernmost North Pacific station (Station ALOHA) in intermediate to deep waters (supporting Fig. s1), which can be attributed to the proximity to hydrothermal systems (de Villiers, 1998; de Villiers and Nelson, 1999). We analysed magnesium concentrations and $^{87}Sr/^{86}Sr$ for these samples because a hydrothermal source would have no magnesium and have lower $^{87}Sr/^{86}Sr$ (0.703–0.705) (Albarède et al., 1981; Krabbenhöft et al., 2010) than the value of 0.709179 ± 0.000002 reported for seawater samples from various locations (Mokadem et al., 2015). The $^{87}Sr/^{86}Sr$ data for samples from Station ALOHA yield an average value 0.709188 ± 0.000006 (2σ SD, $n = 11$), while magnesium concentrations at Station ALOHA are constant at 52.86 ± 0.13 mmol kg^{-1} (2σ SD, $n = 23$) (Fig. 5). These values, which are so close to those of normal seawater, suggest that the Ca_{ex} anomaly, if genuine, is not due to hydrothermal activity near Station ALOHA.

Salinity-normalized calcium and A_T in surface water along the path between the entry point of Indian Ocean surface waters to the Red Sea (Straits of Bab-el-Mandeb) and the Red Sea at 24°N decrease at the ratio expected for net $CaCO_3$ precipitation (Fig. 6A; Steiner et al., 2018). In

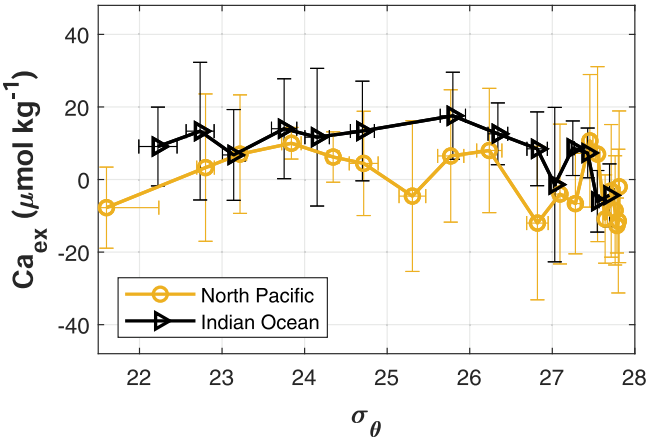

Fig. 2. Potential-density-averaged Ca_{ex} for the studied ocean sections. Samples from each transect were averaged according to their potential density range, at σ_θ intervals of 0.5 until 27.0 and narrower intervals above. Horizontal error bars indicate $\pm 1\sigma$ SD of the potential density of the samples averaged into each data point, vertical error bars are $\pm 1\sigma$ SD of the Ca_{ex} of the samples averaged over the potential density interval.

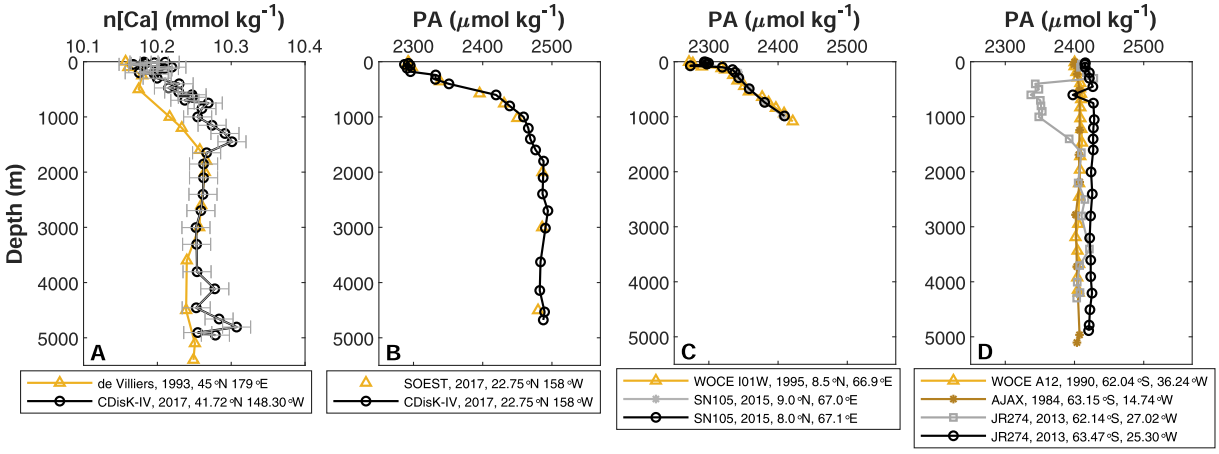

Fig. 3. Comparison of data from this and past studies. The legends depict the cruise name or source, year of sample retrieval, and coordinates. A) Salinity-normalized dissolved calcium concentrations in the North Pacific Ocean, comparing data from de Villiers (1998) and cruise CDisK–IV. Error bars on the CDisK-IV data are ±1σ SD of the analytical method. B) Potential alkalinity at Station ALOHA calculated using August 2017 data from Hawaii Ocean Time-Series (http://aco-ssds.soest.hawaii.edu/ALOHA/) and the present study. C) Comparison of Indian Ocean potential alkalinity calculated using data from cruise SN105 and WOCE data (Johnson et al., 2002) downloaded from GLODAPv2.2020 (Olsen et al., 2020). The grey line in C is hidden by the black line. D) Comparison of Weddell Sea (Southern Ocean) potential alkalinity calculated from cruise JR274 data (Stations 43 & 44), and two past cruises, Station 129 from WOCE transect A12 (Chipman et al., 1994) and Station 96 from AJAX cruise leg 2 (Chipman et al., 1986), downloaded from GLODAPv2.2020 data (Olsen et al., 2020). Analytical error bars for alkalinity determination are normally smaller than the symbol size.

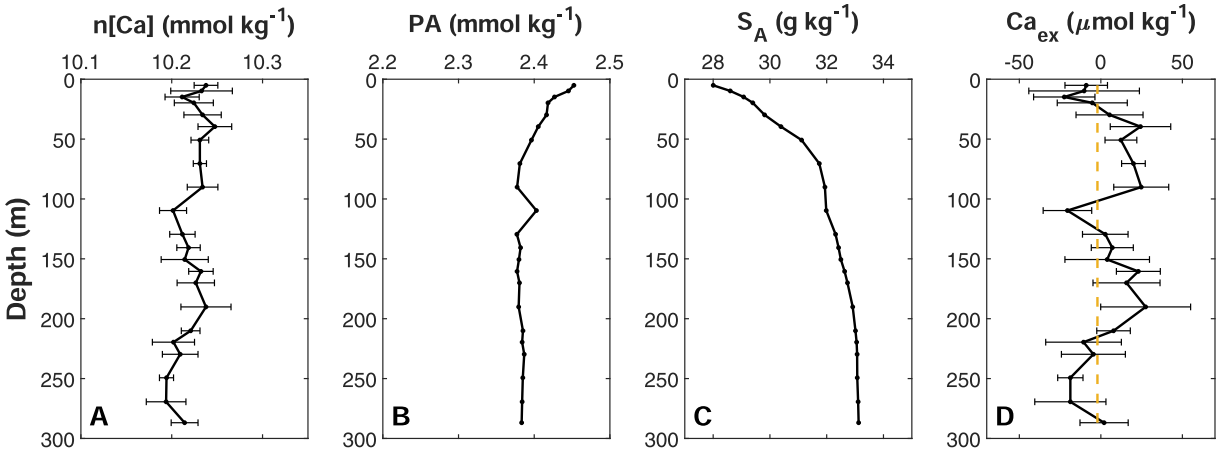

Fig. 4. Salinity-normalized calcium concentrations, potential alkalinity, absolute salinity and excess calcium in Resurrection Bay, a fjord on the coast of Alaska. Error bars mark the average difference between duplicate analyses of calcium concentrations in A, and the resulting uncertainty in calculation of Ca_{ex} in D. The dashed line in D marks the average Ca_{ex} of all open ocean samples from the North Pacific cruise.

samples collected during wintertime, the trend in n[Ca]-to-nA_T concentrations changes northward of 24°N (Fig. 6A). While nA_T continues to decrease in surface waters of the northern Red Sea, calcium concentrations increase. The regression of northern Red Sea n[Ca]-to-nA_T concentrations is similar to that expected for an idealized hydrothermal source (German and Seyfried, 2014), but there is no statistically significant latitudinal trend in $^{87}Sr/^{86}Sr$ in surface waters of the Red Sea (Fig. 6B). Deeper waters from the northern Red Sea have higher Ca_{ex} by ~85 μmol kg^{-1} than other ocean waters analysed in this study (Fig. 6C).

5. DISCUSSION

Our study, with more complete global coverage than past studies, suggests there are no significant calcium excess anomalies in the ocean, except for the intermediate waters of the Indian Ocean.

5.1. North Pacific Ocean

Data from the North Pacific transect do not support conclusions of previous studies that suggest wide spread

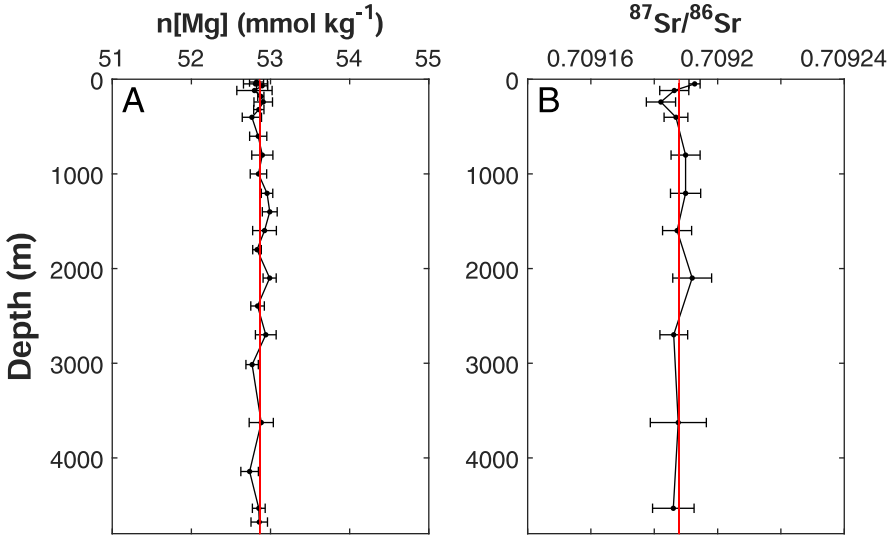

Fig. 5. Salinity-normalized magnesium concentrations (a) and $^{87/86}$Sr isotope ratio (b) at Station ALOHA in the North Pacific. The red lines mark the average magnesium concentration at Station ALOHA and $^{87}Sr/^{86}Sr = 0.709188$. Error bars mark the average difference between duplicate analyses of the samples.

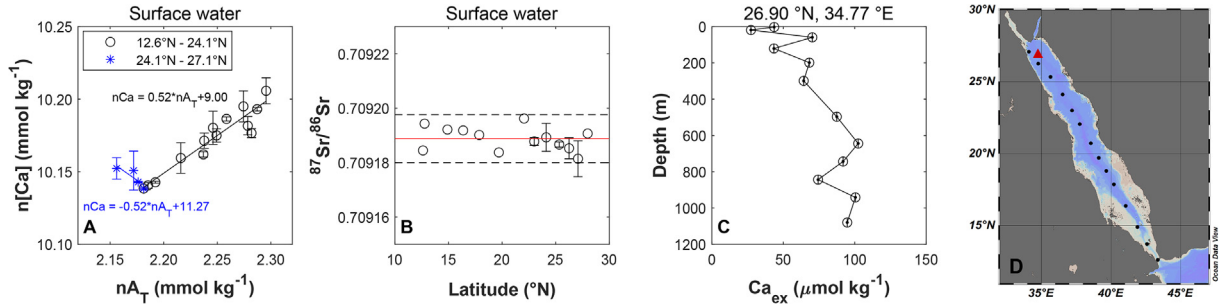

Fig. 6. Red Sea water chemistry. (A) Surface water calcium versus total alkalinity, normalized to absolute salinity of 35 g kg^{-1}, along the main axis of the Red Sea (Data from Steiner et al., 2018). Error bars mark the average difference between duplicate analyses. (B) $^{87/86}$Sr isotope ratio of surface waters along the main axis of the Red Sea. Solid red line marks the average $^{87}Sr/^{86}Sr$ of this data set, dashed lines mark the analytic 2σ SD. (C) Ca_{ex} in a full oceanographic station in the northern Red Sea (Data from Krumgalz and Erez, 1984; Krumgalz et al., 1990). D) location map for the Red Sea samples. Black circles mark surface water samples collected in December 2015–January 2016; a red triangle marks the location of the full oceanographic station plotted in figure C.

excess calcium anomalies (Fig. 2). It may be that there are slight depth variations in Ca_{ex} at the southern and northern most stations of this transect, but radiogenic strontium isotopes as well as magnesium concentrations do not support a large contribution from a hydrothermal source at Station ALOHA (Fig. 5). Evidence for hydrothermal contributions are stronger at Station Papa, where we found stones of igneous composition on core-tops collected during the CDisK-IV cruise, but Ca_{ex} tend toward negative values at Station Papa.

Limited depth variability in Ca_{ex} in the Pacific Ocean suggest that the range of variability in Ca_{ex} caused by variability in the concentrations of organic alkalinity in the open ocean, and export of high-magnesium calcite, is smaller than our uncertainties and goes undetected by our method. This conclusion agrees with those of past studies. Fong and Dickson (2019) calculated a global average variability of ±2 μmol kg^{-1} of organic alkalinity in the open ocean, variability that is smaller than the uncertainty in determination of Ca_{ex}, and would go undetected in the present study. Production of high-magnesium calcite might change calcium to A_T ratios but is normally restricted to benthic communities, as pelagic calcareous plankton build their skeletons from low-magnesium calcite or aragonite (Milliman, 1974). In the open ocean, high-magnesium calcite can form in fish guts, yet most of the fish high-magnesium calcite is soluble at the depth of formation (Wilson et al., 2009; Woosley et al., 2012), and therefore does not create Ca_{ex} anomalies.

de Villiers (1998) suggested that there is an increase in calcium concentrations relative to A_T in the Pacific Ocean at the depth range 1500–4000 m as AABW flows northward. Calcium concentrations measured in the present and in de Villiers's study agree well at the depth range 1600–3400 m (Fig. 3a), and the difference between the results of the two studies arises mostly from the selection of a different Southern Ocean end-member for calculations of Ca_{ex}. de Villiers (1998) did not collect samples from the

Southern Ocean, their choice of calcium and PA was based on results of past studies. A comparison of our Southern Ocean data with their choice of the Southern Ocean end-member suggests that the calcium concentration they cited was too low.

We assume that the Southern Ocean is the source for nearly all North Pacific water. Local water masses such as the North Pacific Intermediate Water form internally within the basin, and our analyses of Alaskan water does not suggest a source that would modify Ca_{ex} of the open waters by a measurable amount.

5.2. A Red Sea origin for excess calcium in the Indian Ocean

We suggest that part of the Ca_{ex} anomaly found in shallow to intermediate waters of the North Indian Ocean originates in the Red Sea. This is because the anomaly is more persistent north of the equator and centres at ~750 m, where the Red Sea water mass of the Indian Ocean is expected. This claim is supported by the existence of a corresponding salinity anomaly.

Water circulation at the shallow Straits of Bab-el-Mandeb, connecting the Red Sea and Indian Ocean, is typical inverse-estuarine during most of the year. When Gulf of Aden surface water flows into the Red Sea, intermediate Red Sea water flows beneath it in the opposite direction; during summer there is a reversal in surface flow direction and formation of a three-layer flow structure (Sofianos and Johns, 2002; Yao et al., 2014a; Yao et al., 2014b). Upon entering the Gulf of Aden, high salinity Red Sea water sinks to depths of a few hundred meters and spreads laterally in the northern Indian Ocean (Rochford, 1964; Wyrtki, 1973; You and Tomczak, 1993; Beal et al., 2000). To assess whether there is a substantial Ca_{ex} anomaly carried from the Red Sea to the Indian Ocean, we re-evaluate oceanographic data from 1982 (Krumgalz and Erez, 1984; Krumgalz et al., 1990), when calcium and A_T concentrations were last measured in depth transects along the Red Sea. The Krumgalz and Erez data show that there was a substantial Ca_{ex} anomaly in the intermediate and deep waters of the northern Red Sea (Fig. 6C).

The northern Red Sea is a site of deep-water formation in winter (Sofianos and Johns, 2003; Yao et al., 2014a). Based on the physical oceanography of the basin and hydrothermal like n[Ca]-to-nA_T ratios of the northern Red Sea surface water (Fig. 6A), Steiner et al. (2018) postulated that some abyssal brine water from the Red Sea makes its way to the surface during winter mixing. This hypothesis is supported by reports of magnesium depletion in the Red Sea water mass of the Indian Ocean (Sen Gupta and Naqvi, 1984) and in the northern Red Sea (Steiner et al., 2014). In addition to an expected increase in calcium concentrations and decreases in salinity-normalized magnesium and A_T concentrations, a hydrothermal source should also decrease $^{87}Sr/^{86}Sr$ of seawater, as discussed for the North Pacific case. Our analyses of the $^{87}Sr/^{86}Sr$ in Red Sea surface water samples yield an average $^{87}Sr/^{86}Sr = 0.709189 \pm 0.000008$ (2σ SD, $n = 13$), similar to values measured in the North Pacific, with no evidence for systemic variations from the average (Fig. 6B). This suggests that there is no substantial hydrothermal source in the Red Sea or North Pacific.

It is thus apparent that Ca_{ex} data from the Red Sea support a deep-sea source for the anomaly (Fig. 6 A&C) while the analytically more precise analysis of radiogenic strontium isotopes does not support mixing of water from a hydrothermal source with Red Sea surface waters (Fig. 6B). These two observations are reconciled because geochemical studies of Red Sea hot brines have shown that Red Sea brine water, including its strontium, is mostly derived from rock formations precipitated during the Miocene, rather than hydrothermal fluids (Zierenberg and Shanks, 1986; Pierret et al., 2001). This suggests that the origin of the Ca_{ex} anomaly is dissolution of Messinian gypsum from the thick evaporite layers found in the Red Sea subsurface during recirculation of Red Sea water through the sediment (Fig. 7).

The Red Sea bottom is dotted with hot and saline brines. Danielsson et al. (1980) measured salinities up to 250 in two of these brines, Atlantis II and Discovery (6.2 times deep Red Sea salinity). Brine alkalinities were similar to the deep-water A_T, and calcium concentrations were ten times that of deep Red Sea water. If these numbers are representative of the entire Red Sea, subterranean discharge provides water that is both high in calcium and low in A_T relative to salinity-normalized seawater. Normalized to salinity of 35 g kg^{-1}, the composition of this source is $[Ca] \approx 16.5$ mmol kg^{-1} and $[PA] \approx 0.31$ mmol kg^{-1}. Mixing of limited quantities of this end-member with water that has initial $n[Ca] = 10.15$ mmol kg^{-1} and $[PA] = 2.14$ mmol kg^{-1} would roughly decrease PA by 1 unit per 3 units of added calcium. We have measured excess calcium anomalies of 15 ± 7 µmol kg^{-1} (95% confidence interval) in the intermediate waters along the Indian Ocean transect, compared with deeper water from the same transect (Fig. 2), suggesting that the PA should be corrected by addition of $2 * (15 \pm 7)/3 = 10 \pm 5$ µmol kg^{-1} to measured values.

The upward correction to the Indian Ocean PA data suggests that $CaCO_3$ dissolution rates at 500–900 m in the northern Indian Ocean are underestimated using directly measured A_T. However, this correction can be ignored if calculations consider the low initial salinity-normalized A_T of the Red Sea and Persian Gulf outflow waters. The best attempts to calculate water column $CaCO_3$ dissolution rates using A_T data assumed preformed A_T that was calculated as a function of salinity, potential temperature, nutrients and oxygen concentrations (Sabine et al., 2002; Feely et al., 2004). With this assumed preformed endmember, it was calculated that $CaCO_3$ dissolution contributes about 10 µmol kg^{-1} of A_T at ~700 m in the North Indian Ocean. If preformed PA of mixed Indian Ocean – Red Sea water is ~10 µmol kg^{-1} lower than assumed from global ocean concentrations, water column $CaCO_3$ dissolution rates at 500–900 m in the northern Indian Ocean were previously underestimated by a factor of two. This depth range lies at and below the aragonite saturation horizon, hence the significance of the correction is that the amount of aragonite dissolved along the northern Indian Ocean water column is similar to the amount of calcite dissolved in this

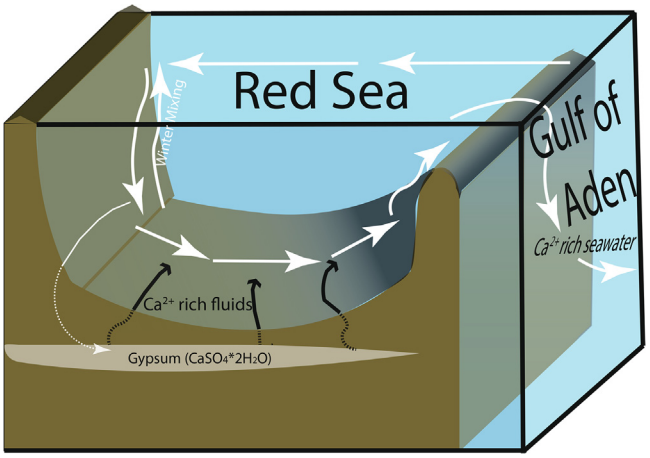

Fig. 7. Schematic illustration of the process enriching Red Sea water in calcium and propagation of this enrichment to the North Indian Ocean.

region, or that much more calcite dissolves in supersaturated waters than previously assumed.

6. SUMMARY

Stability of Ca_{ex} in most of the global ocean suggests that, in most cases, use of potential alkalinity or calcium concentrations for calculation of $CaCO_3$ precipitation and dissolution rates provide similar results. Persistently anomalous Ca_{ex} was found in the intermediate to shallow waters of the North Indian Ocean. In the Indian Ocean, high Ca_{ex} anomalies are directly linked to the formation of unusual intermediate water masses to the north, which are influenced by input of calcium to bottom waters in contact with subsurface gypsum deposits.

Declaration of Competing Interest

The authors declare that they have no known competing financial interests or personal relationships that could have appeared to influence the work reported in this paper.

ACKNOWLEDGEMENTS

This study was funded by a Blavatnik postdoctoral fellowship to ZS, an Isaac Newton Trust grant to AVT and ZS, and ERC StG 307582 (CARBONSINK) to AVT. The cruise on board the ORV Sagar Nidhi was funded by the Indian National Centre for Ocean Information Services (INCOIS), Ministry of Earth Sciences, India, as the first cruise of the second International Indian Ocean Expedition (IIOE-2). The cruise on board the RV Kilo Moana was funded by NSF Ocean Acidification grant number OCE1220600. We would like to thank the UK Natural Environment Research Council (NERC), the UK Department of Environment, Food and Rural Affairs (DEFRA), and the UK Department of Energy and Climate Change (DECC) for funding the research cruise JR274 via the pelagic consortium of UK Ocean Acidification research programme (grant no. NE/H017348/1) and the UK Carbonate Chemistry Facility. We thank Jonathan Erez, Boaz Lazar and Murielle Dray for enabling ZS to measure A_T and salinity in their labs, and Loraine Martell-Bonet for analysing total alkalinity during CDisK-IV. The manuscript benefited greatly from the comments and remarks of Alfonso Mucci and three anonymous reviewers.

APPENDIX A. SUPPLEMENTARY MATERIAL

Supplementary data to this article can be found online at https://doi.org/10.1016/j.gca.2021.03.027.

REFERENCES

Albarède F., Michard A., Minster J. F. and Michard G. (1981) $^{87}Sr/^{86}Sr$ ratios in hydrothermal waters and deposits from the East Pacific Rise at 21°N. *Earth Planet. Sci. Lett.* **55**, 229–236.

Archer D., Eby M., Brovkin V., Ridgwell A., Cao L., Mikolajewicz U., Caldeira K., Matsumoto K., Munhoven G., Montenegro A. and Tokos K. (2009) Atmospheric lifetime of fossil fuel carbon dioxide. *Ann. Rev. Earth Planet. Sci. Ann. Rev. Palo Alto*, 117–134.

Beal L. M., Ffield A. and Gordon A. L. (2000) Spreading of Red Sea overflow waters in the Indian Ocean. *J. Geophys. Res.-Oceans* **105**, 8549–8564.

Beckwith S. T., Byrne R. H. and Hallock P. (2019) Riverine calcium end-members improve coastal saturation state calculations and reveal regionally variable calcification potential. *Front. Mar. Sci.* **6**.

Berelson W. M., Balch W. M., Najjar R., Feely R. A., Sabine C. and Lee K. (2007) Relating estimates of $CaCO_3$ production, export, and dissolution in the water column to measurements of $CaCO_3$ rain into sediment traps and dissolution on the sea floor: A revised global carbonate budget. *Glob. Biogeochem. Cycle* **21**, 15.

Betzer P. R., Byrne R. H., Acker J. G., Lewis C. S., Jolley R. R. and Feely R. A. (1984) The oceanic carbonate system: A reassessment of biogenic controls. *Science* **226**, 1074–1077.

Bishop J. K. B., Edmond J. M., Ketten D. R., Bacon M. P. and Silker W. B. (1977) The chemistry, biology, and vertical flux of particulate matter from the upper 400 m of the equatorial Atlantic Ocean. *Deep Sea Res.* **24**, 511–548.

Bishop J. K. B., Ketten D. R. and Edmond J. M. (1978) The chemistry, biology and vertical flux of particulate matter from the upper 400 m of the Cape Basin in the southeast Atlantic Ocean. *Deep Sea Res.* **25**, 1121–1161.

Boudreau B. P., Sulpis O. and Mucci A. (2020) Control of $CaCO_3$ dissolution at the deep seafloor and its consequences. *Geochim. Cosmochim. Acta* **268**, 90–106.

Brewer P. G., Wong G. T. F., Bacon M. P. and Spencer D. W. (1975) An oceanic calcium problem? Earth Planet. *Sci. Lett.* **26**, 81–87.

Buitenhuis E. T., Le Quéré C., Bednaršek N. and Schiebel R. (2019) Large Contribution of Pteropods to Shallow $CaCO_3$ Export. *Glob. Biogeochem. Cycle* **33**, 458–468.

Byrne R. H., Acker J. G., Betzer P. R., Feely R. A. and Cates M. H. (1984) Water column dissolution of aragonite in the Pacific Ocean. *Nature* **312**, 321–326.

Cao Z. M. and Dai M. H. (2011) Shallow-depth $CaCO_3$ dissolution: Evidence from excess calcium in the South China Sea and its export to the Pacific Ocean. *Glob. Biogeochem. Cycle* **25**.

Chakrabarti R., Mondal S., Acharya S. S., Lekha J. S. and Sengupta D. (2018) Submarine groundwater discharge derived strontium from the Bengal Basin traced in Bay of Bengal water samples. *Sci. Rep.* **8**.

Chipman D. W., Takahashi T., Breger D. and Sutherland S. C. (1994) *Carbon Dioxide, Hydrographic, and Chemical Data Obtained During the R/V Meteor Cruise 11/5 in the South Atlantic and Northern Weddell Sea Areas (WOCE sections A-12 and A-21). ORNL/CDIAC-55, NDP-045*. Carbon Dioxide Information Analysis Center, Oak Ridge National Laboratory, U.S. Department of Energy, Oak Ridge, Tennessee.

Chipman D. W., Takahashi T. and Sutherland S. C. (1986) *Carbon chemistry of the South Atlantic Ocean and the Weddell Sea: The results of the Atlantic Long Lines (AJAX) expeditions, October, 1983 - February, 1985*. LDGO, p. 185.

Craig H. (1966) Isotopic composition and origin of the Red Sea and Salton Sea geothermal brines. *Science* **154**, 1544–1548.

de Villiers S. (1998) Excess dissolved Ca in the deep ocean: a hydrothermal hypothesis. *Earth Planet. Sci. Lett.* **164**, 627–641.

de Villiers S., Greaves M. and Elderfield H. (2002) An intensity ratio calibration method for the accurate determination of Mg/Ca and Sr/Ca of marine carbonates by ICP-AES. *Geochem. Geophys. Geosyst.*, 3.

de Villiers S. and Nelson B. K. (1999) Detection of low-temperature hydrothermal fluxes by seawater Mg and Ca anomalies. *Science* **285**, 721–723.

Dickson A. G. (1981) An exact definition of total alkalinity and a procedure for the estimation of alkalinity and total inorganic carbon from titration data. Deep Sea Research Part A. *Oceanogr. Res. Pap.* **28**, 609–623.

Doney S. C., Fabry V. J., Feely R. A. and Kleypas J. A. (2009) Ocean acidification: The other CO_2 problem. *Ann. Rev. Mar. Sci.* **1**, 169–192.

Feely R. A., Sabine C. L., Lee K., Berelson W., Kleypas J., Fabry V. J. and Millero F. J. (2004) Impact of anthropogenic CO_2 on the $CaCO_3$ system in the oceans. *Science* **305**, 362–366.

Feely R. A., Sabine C. L., Lee K., Millero F. J., Lamb M. F., Greeley D., Bullister J. L., Key R. M., Peng T. H., Kozyr A., Ono T. and Wong C. S. (2002) In situ calcium carbonate dissolution in the Pacific Ocean. *Glob. Biogeochem. Cycle* **16**, 91–1.

Fong M. B. and Dickson A. G. (2019) Insights from GO-SHIP hydrography data into the thermodynamic consistency of CO_2 system measurements in seawater. *Mar. Chem.* **211**, 52–63.

Friis K., Körtzinger A. and Wallace D. W. R. (2003) The salinity normalization of marine inorganic carbon chemistry data. *Geophys. Res. Lett.* **30**(2).

Froelich P. N., Klinkhammer G. P., Bender M. L., Luedtke N. A., Heath G. R., Cullen D., Dauphin P., Hammond D., Hartman B. and Maynard V. (1979) Early oxidation of organic matter in pelagic sediments of the eastern equatorial Atlantic: Suboxic diagenesis. *Geochim. Cosmochim. Acta* **43**, 1075–1090.

Fry C. H., Tyrrell T., Hain M. P., Bates N. R. and Achterberg E. P. (2015) Analysis of global surface ocean alkalinity to determine controlling processes. *Mar. Chem.* **174**, 46–57.

German C. R. and Seyfried W. E. (2014) Hydrothermal Processes. In *Treatise on Geochemistry* (eds. H. D. Holland and K. K. Turekian), second ed. Elsevier, Oxford, pp. 191–233.

Gruber N., Clement D., Carter B. R., Feely R. A., van Heuven S., Hoppema M., Ishii M., Key R. M., Kozyr A., Lauvset S. K., Lo Monaco C., Mathis J. T., Murata A., Olsen A., Perez F. F., Sabine C. L., Tanhua T. and Wanninkhof R. (2019) The oceanic sink for anthropogenic CO_2 from 1994 to 2007. *Science* **363**, 1193–1199.

Honjo S., Manganini S. J., Krishfield R. A. and Francois R. (2008) Particulate organic carbon fluxes to the ocean interior and factors controlling the biological pump: A synthesis of global sediment trap programs since 1983. *Prog. Oceanogr.* **76**, 217–285.

Horibe Y., Endo K. and Tsubota H. (1974) Calcium in the South Pacific, and its correlation with carbonate alkalinity. *Earth Planet. Sci. Lett.* **23**, 136–140.

Ilyina T. and Zeebe R. E. (2012) Detection and projection of carbonate dissolution in the water column and deep-sea sediments due to ocean acidification. *Geophys. Res. Lett.* **39**, 6.

IOC, SCOR and IAPSO (2010) The international thermodynamic equation of seawater – 2010: Calculation and use of thermodynamic properties, Intergovernmental Oceanographic Commission, Manuals and Guides No. 56, p. 196. http://www.TEOS-10.org.

Jansen H., Zeebe R. E. and Wolf-Gladrow D. A. (2002) Modeling the dissolution of settling $CaCO_3$ in the ocean. *Glob. Biogeochem. Cycle* **16**, 16.

Jiang Z.-P., Tyrrell T., Hydes D. J., Dai M. and Hartman S. E. (2014) Variability of alkalinity and the alkalinity-salinity relationship in the tropical and subtropical surface ocean. *Glob. Biogeochem. Cycle* **28**, 729–742.

Johnson K. M., Dickson A. G., Eischeid G., Goyet C., Guenther P. R., Key R. M., Lee K., Lewis E. R., Millero F. J., Purkerson D., Sabine C. L., Schottle R. G., Wallace D. W. R., Wilke R. J. and Winn C. D. (2002) Carbon Dioxide, Hydrographic and Chemical Data Obtained During the Nine R/V Knorr Cruises Comprising the Indian Ocean CO2 Survey (WOCE Sections I8SI9S, I9N, I8NI5E, I3, I5WI4, I7N, I1, I10, and I2; December 1, 1994 - January 22, 1996). In *ORNL/CDIAC-138, NDP-080* (ed. A. Kozyr). Carbon Dioxide Information Analysis Center, Oak Ridge National Laboratory, U.S. Department of Energy, Oak Ridge, Tennessee.

Kanamori S. and Ikegami H. (1982) Calcium-alkalinity relationship in the North Pacific. *J. Oceanogr. Soc. Jpn.* **38**, 57–62.

Keil R. (2017) Anthropogenic forcing of carbonate and organic carbon preservation in marine sediments. *Ann. Rev. Mar. Sci.* **9**, 151–172.

Kirkwood D. (1996) Nutrients: Practical notes on their determination in sea water. p. 25.

Ko Y. H., Lee K., Eom K. H. and Han I.-S. (2016) Organic alkalinity produced by phytoplankton and its effect on the computation of ocean carbon parameters. *Limnol. Oceanogr.* **61**, 1462–1471.

Krabbenhöft A., Eisenhauer A., Böhm F., Vollstaedt H., Fietzke J., Liebetrau V., Augustin N., Peucker-Ehrenbrink B., Müller M. N., Horn C., Hansen B. T., Nolte N. and Wallmann K. (2010) Constraining the marine strontium budget with natural strontium isotope fractionations ($^{87}Sr/^{86}Sr^{*}$, $\delta^{88/86}Sr$) of carbonates, hydrothermal solutions and river waters. *Geochim. Cosmochim. Acta* **74**, 4097–4109.

Krumgalz B. S. (1982) Calcium distribution in the world ocean waters. *Oceanol. Acta* **5**, 121–128.

Krumgalz B. S. and Erez J. (1984) Chemical oceanography survey of the northern Red Sea, the straits of Tiran and the Gulf of Elat, I.O.L.R. reports, series H, Haifa. p. 133.

Krumgalz B. S., Erez J. and Chen C. T. A. (1990) Anthropogenic CO_2 penetration in the northern Red Sea and in the Gulf of Elat (Aqaba). *Oceanol. Acta* **13**, 283–290.

Kürten B., Zarokanellos N. D., Devassy R. P., El-Sherbiny M. M., Struck U., Capone D. G., Schulz I. K., Al-Aidaroos A. M., Irigoien X. and Jones B. H. (2019) Seasonal modulation of mesoscale processes alters nutrient availability and plankton communities in the Red Sea. *Prog. Oceanogr.* **173**, 238–255.

Lebrato M., Garbe-Schönberg D., Müller M. N., Blanco-Ameijeiras S., Feely R. A., Lorenzoni L., Molinero J.-C., Bremer K., Jones D. O. B., Iglesias-Rodriguez D., Greeley D., Lamare M. D., Paulmier A., Graco M., Cartes J., Barcelos e Ramos J., de Lara A., Sanchez-Leal R., Jimenez P., Paparazzo F. E., Hartman S. E., Westernströer U., Küter M., Benavides R., da Silva A. F., Bell S., Payne C., Olafsdottir S., Robinson K., Jantunen L. M., Korablev A., Webster R. J., Jones E. M., Gilg O., Bailly du Bois P., Beldowski J., Ashjian C., Yahia N. D., Twining B., Chen X.-G., Tseng L.-C., Hwang J.-S., Dahms H.-U. and Oschlies A. (2020) Global variability in seawater Mg:Ca and Sr:Ca ratios in the modern ocean. *Proc. Natl. Acad. Sci. USA*, 201918943.

Liu X., Byrne R. H., Lindemuth M., Easley R. and Mathis J. T. (2015) An automated procedure for laboratory and shipboard spectrophotometric measurements of seawater alkalinity: Continuously monitored single-step acid additions. *Mar. Chem.* **174**, 141–146.

McDougall T. J. and Barker P. M. (2011) Getting started with TEOS-10 and the Gibbs Seawater (GSW) Oceanographic Toolbox. SCOR/IAPSO WG127. p. 28.

Millero F. J., Feistel R., Wright D. G. and McDougall T. J. (2008) The composition of Standard Seawater and the definition of the Reference-Composition Salinity Scale. *Deep Sea Res. Part I* **55**, 50–72.

Milliman J. D. (1974) *Marine carbonates*. Springer-Verlag, Berlin.

Milliman J. D., Troy P. J., Balch W. M., Adams A. K., Li Y. H. and Mackenzie F. T. (1999) Biologically mediated dissolution of calcium carbonate above the chemical lysocline? *Deep-Sea Res. Part I-Oceanogr. Res. Pap.* **46**, 1653–1669.

Mokadem F., Parkinson I. J., Hathorne E. C., Anand P., Allen J. T. and Burton K. W. (2015) High-precision radiogenic strontium isotope measurements of the modern and glacial ocean: Limits on glacial-interglacial variations in continental weathering. *Earth Planet. Sci. Lett.* **415**, 111–120.

Naqvi S. W. A. and Naik S. (1983) Calcium: chlorinity ratio and carbonate dissolution in the northwestern Indian Ocean. *Deep Sea Res. Part A Oceanogr. Res. Pap.* **30**, 381–392.

Naviaux J. D., Subhas A. V., Dong S., Rollins N. E., Liu X., Byrne R. H., Berelson W. M. and Adkins J. F. (2019) Calcite dissolution rates in seawater: Lab vs. in-situ measurements and inhibition by organic matter. *Mar. Chem.* **215** 103684.

Olsen A., Lange N., Key R. M., Tanhua T., Bittig H. C., Kozyr A., Àlvarez M., Azetsu-Scott K., Becker S., Brown P. J., Carter B. R., Cotrim da Cunha L., Feely R. A., van Heuven S., Hoppema M., Ishii M., Jeansson E., Jutterström S., Landa C. S., Lauvset S. K., Michaelis P., Murata A., Pérez F. F., Pfeil B., Schirnick C., Steinfeldt R., Suzuki T., Tilbrook B., Velo A., Wanninkhof R. and Woosley R. J. (2020) An updated version of the global interior ocean biogeochemical data product, GLODAPv2. 2020. *Earth Syst. Sci. Data* **12**(4), 3653–3678.

Orr J. C., Epitalon J. M., Dickson A. G. and Gattuso J. P. (2018) Routine uncertainty propagation for the marine carbon dioxide system. *Mar. Chem.* **207**, 84–107.

Pierret M. C., Clauer N., Bosch D., Blanc G. and France-Lanord C. (2001) Chemical and isotopic ($^{87}Sr/^{86}Sr$, $\delta^{18}O$, δD) constraints to the formation processes of Red-Sea brines. *Geochim. Cosmochim. Acta* **65**, 1259–1275.

Rochford D. J. (1964) Salinity maxima in the upper 1000 metres of the North Indian Ocean. *Mar. Freshw. Res.* **15**, 1–24.

Roson G., Guallart E. F., Perez F. F. and Rios A. F. (2016) Calcium distribution in the subtropical Atlantic Ocean: Implications for calcium excess and saturation horizons. *J. Mar. Syst.* **158**, 45–51.

Sabine C. L., Feely R. A., Gruber N., Key R. M., Lee K., Bullister J. L., Wanninkhof R., Wong C. S., Wallace D. W. R., Tilbrook B., Millero F. J., Peng T. H., Kozyr A., Ono T. and Rios A. F. (2004) The oceanic sink for anthropogenic CO_2. *Science* **305**, 367–371.

Sabine C. L., Key R. M., Feely R. A. and Greeley D. (2002) Inorganic carbon in the Indian Ocean: Distribution and dissolution processes. *Glob. Biogeochem. Cycle* **16**.

Sass E. and Ben-Yaakov S. (1977) The carbonate system in hypersaline solutions: Dead Sea brines. *Mar. Chem.* **5**, 183–199.

Schlitzer R. (2020) Ocean Data View.

Schlosser C., Schmidt K., Aquilina A., Homoky W. B., Castrillejo M., Mills R. A., Patey M. D., Fielding S., Atkinson A. and Achterberg E. P. (2018) Mechanisms of dissolved and labile particulate iron supply to shelf waters and phytoplankton blooms off South Georgia, Southern Ocean. *Biogeosciences* **15**, 4973–4993.

Schrag D. P. (1999) Rapid analysis of high-precision Sr/Ca ratios in corals and other marine carbonates. *Paleoceanography* **14**, 97–102.

Sen Gupta R., Naik S. and Singbal S. Y. S. (1978) A study of fluoride, calcium and magnesium in the Northern Indian Ocean. *Mar. Chem.* **6**, 125–141.

Sen Gupta R. and Naqvi S. W. A. (1984) Chemical oceanography of the Indian Ocean, north of the equator. *Deep Sea Res. Part A Oceanogr. Res. Pap.* **31**, 671–706.

Shiller A. M. and Gieskes J. M. (1980) Processes affecting the oceanic distributions of dissolved calcium and alkalinity. *J. Geophys. Res. Oceans* **85**, 2719–2727.

Sofianos S. S. and Johns W. E. (2002) An Oceanic General Circulation Model (OGCM) investigation of the Red Sea circulation, 1. Exchange between the Red Sea and the Indian Ocean. *J. Geophys. Res.-Oceans* **107**, 11.

Sofianos S. S. and Johns W. E. (2003) An Oceanic General Circulation Model (OGCM) investigation of the Red Sea circulation: 2. Three-dimensional circulation in the Red Sea. *J. Geophys. Res.-Oceans* **108**, 15.

Steiner Z., Erez J., Shemesh A., Yam R., Katz A. and Lazar B. (2014) Basin-scale estimates of pelagic and coral reef calcification in the Red Sea and Western Indian Ocean. *Proc. Natl. Acad. Sci. USA* **111**, 16303–16308.

Steiner Z., Lazar B., Reimers C. E. and Erez J. (2019) Carbonates dissolution and precipitation in hemipelagic sediments overlaid by supersaturated bottom-waters - Gulf of Aqaba. *Red Sea. Geochim. Cosmochim. Acta* **246**, 565–580.

Steiner Z., Sarkar A., Prakash S., Vinayachandran P. N. and Turchyn A. V. (2020) Dissolved strontium, Sr/Ca ratios, and the abundance of Acantharia in the Indian and Southern Oceans. *ACS Earth Space Chem.* **4**, 802–811.

Steiner Z., Turchyn A. V., Harpaz E. and Silverman J. (2018) Water chemistry reveals a significant decline in coral calcification rates in the southern Red Sea. *Nat. Commun.* **9**, 3615.

Subhas A. V., Adkins J. F., Rollins N. E., Naviaux J., Erez J. and Berelson W. M. (2017) Catalysis and chemical mechanisms of calcite dissolution in seawater. *Proc. Natl. Acad. Sci. USA* **114**, 8175–8180.

Sulpis O., Boudreau B. P., Mucci A., Jenkins C., Trossman D. S., Arbic B. K. and Key R. M. (2018) Current $CaCO_3$ dissolution at the seafloor caused by anthropogenic CO_2. *Proc. Natl. Acad. Sci. USA* **115**, 11700–11705.

Sulpis O., Lix C., Mucci A. and Boudreau B. P. (2017) Calcite dissolution kinetics at the sediment-water interface in natural seawater. *Mar. Chem.* **195**, 70–83.

Takahashi T., Sutherland S. C., Chipman D. W., Goddard J. G., Ho C., Newberger T., Sweeney C. and Munro D. R. (2014) Climatological distributions of pH, pCO_2, total CO_2, alkalinity, and $CaCO_3$ saturation in the global surface ocean, and temporal changes at selected locations. *Mar. Chem.* **164**, 95–125.

Tsunogai S., Yamahata H., Kudo S. and Saito O. (1973) Calcium in the Pacific Ocean. *Deep-Sea Res.* **20**, 717–726.

Tynan E., Clarke J. S., Humphreys M. P., Ribas-Ribas M., Esposito M., Rérolle V. M. C., Schlosser C., Thorpe S. E., Tyrrell T. and Achterberg E. P. (2016) Physical and biogeochemical controls on the variability in surface pH and calcium carbonate saturation states in the Atlantic sectors of the Arctic and Southern Oceans. *Deep Sea Res. Part II* **127**, 7–27.

Wafar M., Qurban M. A., Ashraf M., Manikandan K. P., Flandez A. V. and Balala A. C. (2016) Patterns of distribution of inorganic nutrients in Red Sea and their implications to primary production. *J. Mar. Syst.* **156**, 86–98.

Wilson R. W., Millero F. J., Taylor J. R., Walsh P. J., Christensen V., Jennings S. and Grosell M. (2009) Contribution of fish to the marine inorganic carbon cycle. *Science* **323**, 359.

Wolf-Gladrow D. A., Zeebe R. E., Klaas C., Körtzinger A. and Dickson A. G. (2007) Total alkalinity: The explicit conservative expression and its application to biogeochemical processes. *Mar. Chem.* **106**, 287–300.

Woosley R. J., Millero F. J. and Grosell M. (2012) The solubility of fish-produced high magnesium calcite in seawater. *J. Geophys. Res. Oceans* **117**.

Wyrtki K. (1973) Physical Oceanography of the Indian Ocean. In *The Biology of the Indian Ocean* (eds. B. Zeitzschel and S. A. Gerlach). Springer, Berlin, Heidelberg, pp. 18–36.

Yang B., Byrne R. H. and Lindemuth M. (2015) Contributions of organic alkalinity to total alkalinity in coastal waters: A spectrophotometric approach. *Mar. Chem.* **176**, 199–207.

Yao F., Hoteit I., Pratt L. J., Bower A. S., Koehl A., Gopalakrishnan G. and Rivas D. (2014a) Seasonal overturning circulation in the Red Sea: 2. Winter circulation. *J. Geophys. Res.-Oceans* **119**, 2263–2289.

Yao F., Hoteit I., Pratt L. J., Bower A. S., Zhai P., Koehl A. and Gopalakrishnan G. (2014b) Seasonal overturning circulation in the Red Sea: 1. Model validation and summer circulation. *J. Geophys. Res.-Oceans* **119**, 2238–2262.

You Y. and Tomczak M. (1993) Thermocline circulation and ventilation in the Indian Ocean derived from water mass analysis. *Deep-Sea Res. Part I-Oceanogr. Res. Pap.* **40**, 13–56.

Zierenberg R. A. and Shanks W. C. (1986) Isotopic constraints on the origin of the Atlantis II, Suakin and Valdivia brines. *Red Sea. Geochim. Cosmochim. Acta* **50**, 2205–2214.

Associate editor: Alfonso Mucci